dc conductivity of strong and weak electron spin-orbit scattering materials near the metal-insulator transition

M. Osofsky, H. Tardy, M. LaMadrid, and J. M. Mochel
Materials Research Laboratory and Department of Physics, University of Illinois at Urbana-Champaign, 1110 West Green Street, Urbana, Illinois 61801
(Received 15 February 1985)

A detailed comparison of two disordered alloys, Ge_xAu_{1-x} and B_xCu_{1-x}, is carried out near their metal-insulator transition in zero magnetic field. Ge_xAu_{1-x}, a high-Z material, has been shown to exhibit strong spin-orbit effects in a magnetic field, while B_xCu_{1-x}, a low-Z material, has been shown to exhibit weak spin-orbit effects. Both materials have similar temperature-dependent dc conductivity behavior in zero field and approximately linear mobility edges.

I. INTRODUCTION

Results of recent experiments[1-12] reveal the importance of both disorder and interaction effects in the metal-insulator transition in three-dimensional disordered systems. Transport measurements[1,2] on a-Si:Nb and a-Si:Au show a linear dependence of zero-temperature conductivity on electron density (the so-called mobility edge) as predicted by Al'tshuler *et al.*[13] and McMillan,[14] while measurements on Si:P (Ref. 3,4) show a square-root dependence as predicted by Grest and Lee (Ref. 15). A significant difference between Si:P and the other systems mentioned is spin-orbit scattering. Silicon and phosphorus have low Z and hence low spin-orbit interaction strengths while niobium and gold are relatively high-Z elements and have high spin-orbit interaction strengths.

We report on dc conductivity measurements on amorphous Ge_xAu_{1-x}, a high-Z material, and amorphous B_xCu_{1-x}, a low-Z material, near the metal-insulator transition. Magnetoresistence (MR) measurements[16] reveal the different spin-orbit scattering behaviors of the two materials. The zero-field transport behaviors of the two materials are shown to be similar and in agreement with the Si:Nb and Si:Au work and the theories mentioned above.

II. EXPERIMENTAL PROCEDURE

Conductivity samples were quench-condensed onto polished $\frac{1}{2}\times\frac{1}{8}$ in.^{2} sapphire substrates at 20 K from independent, resistively heated aluminum oxide boats in a dual-source configuration (Fig. 1). A 0.025-mm gold wire was affixed with flexible silver paint to each of four gold strips which were preevaporated onto each substrate. The relative concentrations of the films were determined from two computer-monitored oscillating quartz-crystal thickness monitors, each of which sees only one of the sources. Before and after each evaporation both thickness monitors were calibrated with a commercial quartz-crystal thickness monitor which was exposed to both sources. This crystal also monitored the film thickness during evaporation.

Transmission electron microscopic (TEM) analysis of unannealed GeAu films showed no structure on length scales larger than the TEM's 15-Å resolution for amorphous materials. X-ray diffraction spectra, taken after each of several anneals, confirmed the films amorphous structure. Figure 2 shows a series of spectra from a 2000-Å film of $Ge_{0.81}Au_{0.19}$ taken on a Norelco powder camera with 0.4° resolution. Each curve is the result of subtracting the spectrum of a clean substrate from that of the film on a substrate. One of these background spectra was taken for each sample spectrum. The unannealed film's spectrum (a, Fig. 2) has a maximum at ~28°—30° that is greater than 10° wide. We find crystallites that are approximately 10 Å in diameter from the diffraction rela-

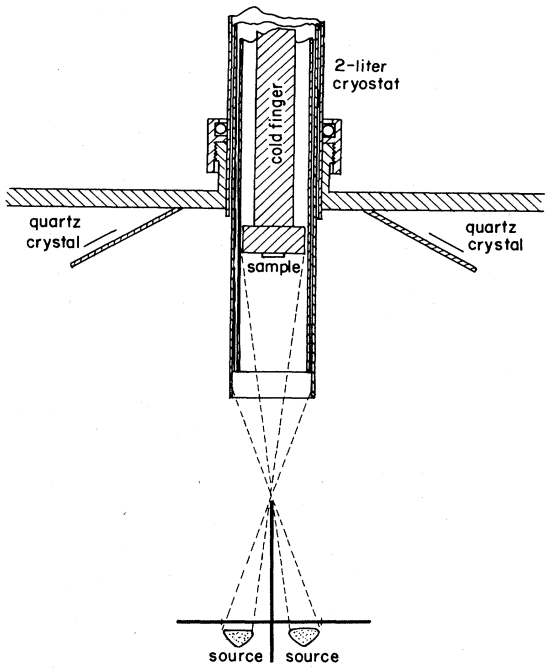

FIG. 1. Dual-source evaporation configuration. Each quartz-crystal thickness monitor sees one source. A calibrated commercial crystal monitor, situated perpendicular to the plane of the figure, calibrates the others and monitors film thickness during evaporation.

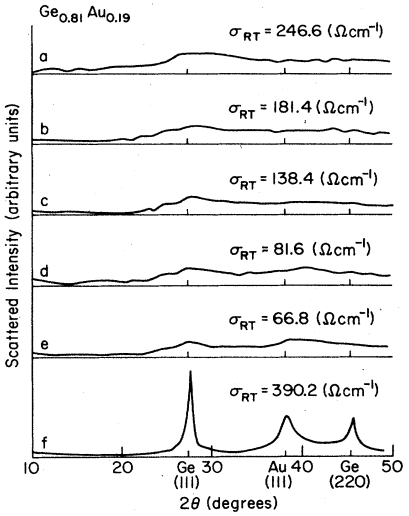

FIG. 2. X-ray diffraction spectra of a 2000-Å $Ge_{0.81}Au_{0.19}$ film as a function of anneal: *a*, after the film was at room temperature for a week; *b*, condition *a* plus 110 °C anneal for 25 min; *c*, condition *b* plus 125 °C anneal for 30 min *d*, condition *c* plus 140 °C anneal for 30 min *e*, condition *d* plus 150 °C anneal for 30 min *f*, condition *e* plus 160 °C anneal for 30 min. Bumps evolve about scattering angles corresponding to Ge and Au crystal peaks as the film's conductivity decreases. At a sample-dependent temperature the film crystallizes and the conductivity increases, *f*.

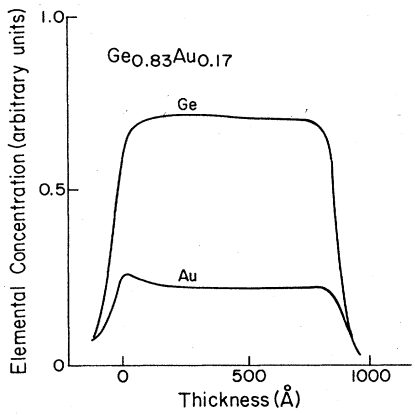

FIG. 3. Variation of elemental concentration versus distance from the substrate for 1000 Å of $Ge_{0.83}Au_{0.17}$. The film's surface is at 1000 Å. The concentrations are constant to within 10%.

tion $D \sim \lambda/\Delta(2\theta)$, where D is the crystallite diameter, λ is the wavelength of the x rays, and $\Delta(2\theta)$ is the width of the peak. This is consistent with the TEM result. After subsequent anneals (*b*—*e*, Fig. 2) very broad peaks form at angles near the Ge(111) and Au(111) crystal peaks. The Ge(111) peak of *e*, Fig. 2, is $\sim 5°$ wide corresponding to a crystallite diameter of about 20 Å. The room-temperature conductivity of the film decreased with each anneal until the anneal at 160 °C for $\frac{1}{2}$ h (*f*, Fig. 2) when the conductivity increased sixfold. The Ge(111) and (220) peaks were then 1° wide corresponding to 90-Å crystallites and the Au(111) peak was 2° wide corresponding to 50-Å crystallites. We model the system as Au atoms, the source of conduction electrons, suspended in an amorphous Ge matrix. The evolution of broad bumps around Ge and Au scattering angles indicates that annealing causes clustering of like atoms in the film. The concurrent decrease in conductivity suggests that Au atoms group into small clusters, reducing the number of conduction electrons and hence reducing the system's Fermi energy. The large conductivity changes accompanied by only small narrowing of the Au bump indicates that the conductivity is very sensitive to Au clustering. At a sample-dependent crystallization temperature, large Ge and Au crystallites form, changing the nature of the system to a random distribution of 90-Å Ge and 60-Å Au crystallites. The system is now ordered on length scales less than 60 Å but amorphous on length scales larger than 100 Å. The Fermi energy increases since the electron density increases with the system's decreased volume, hence the larger conductivity. This decrease in volume must be large enough to overcome the decrease in conduction electrons due to the Au crystallite formation. The film will still behave like an amorphous material since at 4.2 K, our highest temperature, the electrons are coherent up to a length scale of 200 Å. Conduction may also occur along grain boundaries on Au-rich links. This mode of conduction would exhibit percolative or normal two- or three-dimensional metallic behavior depending on the Au concentration and the shapes of the conducting channels. However, the contribution of grain-boundary conduction seems to be negligible since the films exhibit the same amorphous conductivity behavior as the uncrystallized films.

Composition profiles were obtained by combining Auger electron spectroscopy (AES) with sputter etching of the samples. This technique shows the variation in elemental concentration but yields inaccurate absolute concentrations. Figure 3 shows elemental concentration, as determined by AES, as a function of distance from the substrate surface for a 1000-Å film of $Ge_{0.83}Au_{0.17}$. These curves show long-range variations of less than 10% in elemental concentration through each sample. X-ray fluorescence measurements yielded relative concentrations which varied in their agreement with those determined during evaporation from 1% to 20%. This technique is accurate to within 5% as shown by analyzing layered standards. The concentrations presented in this report are those determined by this method. Sample thickness, as measured on an interferometer, agreed with the thickness as determined by the microbalance to within 10%.

The x-ray diffraction spectrum of unannealed $B_{0.81}Cu_{0.19}$ (*a*, Fig. 4) shows no structure above the noise. The spectrum of unannealed $B_{0.68}Cu_{0.32}$ (*c*, Fig. 4) shows a 5° wide peak (corresponding to 20-Å crystallites) at the Cu(111) crystal peak. Annealing these films increased their conductivity. The annealed $B_{0.81}Cu_{0.19}$ (*b*, Fig. 4) spectrum still showed no structure. Annealing the $B_{0.68}Cu_{0.32}$ film (*d*, Fig. 4) narrowed the Cu(111) peak to a width of 2.5°, which corresponds to 40-Å crystallites. A peak also formed at 32°, corresponding to 60-Å boron-

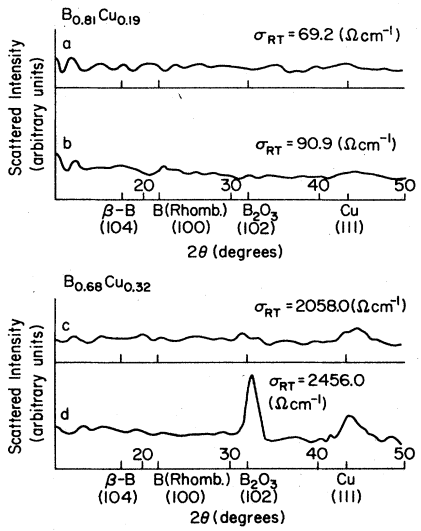

FIG. 4. X-ray diffraction spectra of an 1800-Å $B_{0.81}Cu_{0.19}$ film (*a*, after a day at room temperature and *b*, after a 90 °C anneal) and of a 1700-Å $B_{0.68}Cu_{0.32}$ film (*c*, after a day at room temperature and *d*, after a 90 °C anneal). No crystal structure develops in the Cu dilute film. Cu(111) and B_2O_3 crystal peaks form in the $B_{0.68}Cu_{0.32}$ spectrum. The film conductivity increases with annealing. Further annealing produces little change in conductivity.

oxide crystallites. The pure boron remained amorphous in both annealed films. This behavior can be explained through the presence of voids in the film. These voids increase the separation between the Cu atoms and, hence, lower the Fermi energy. Annealing the film destroys voids which contracts the system and raises the Fermi energy. Again, the contraction must be large enough to overcome the decrease in the number of conduction electrons due to metal crystallite formation. After all of the voids are gone there can be little change in conductivity which is consistent with our experience.

AES analysis (Fig. 5) of a 1000-Å film of $B_{0.83}Cu_{0.17}$ showed B, Cu, and O concentration variations of less than

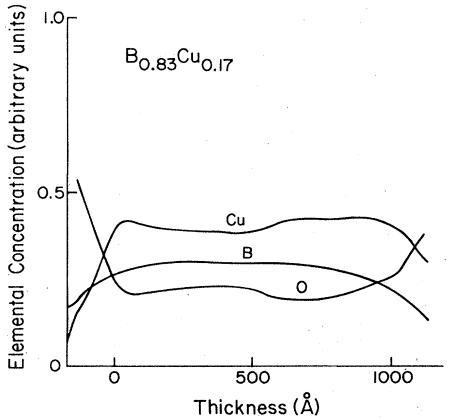

FIG. 5. Variation of elemental concentration versus distance from the substrate for 1000 Å of $B_{0.83}Cu_{0.17}$. The film's surface is at 1000 Å. The concentrations are constant to within 10%.

10% through the sample. The O is due to O liberated from the alumina-coated spiral during evaporation. X-ray fluorescence is insensitive to low-Z elements so this analysis could not be done on this system. The concentrations presented are those determined by the microbalance during evaporation.

As we have seen, the conductivity of the amorphous Ge_xAu_{1-x} decreases with moderate annealing. In fact, a-Ge_xAu_{1-x} approaches and goes through the metal-insulator transition when annealed. We took advantage of this behavior to probe the metal-insulator transition. dc-conductivity data were collected during a series of anneals and measurements. The anneals varied from 50 °C for 20 min to 200 °C for 3 h. We report on data from uncrystallized films. The measurements were taken at room temperature and between 4.2 and 1.5 K. Since annealing B_xCu_{1-x} does not have as strong an effect on the conductivity, this system was driven through the transition by changing composition. A series of samples with $x = 84\%$ to 75% were condensed, warmed to room temperature, and then measured and cooled for the low-temperature measurements.

The low-temperature data were taken with the sample submerged in liquid helium. A manostat controlled the pressure above the helium bath and kept the temperature stable to better than 1%. The temperature of the bath was measured with a germanium resistance thermometer. Four-probe dc-conductivity data were obtained with a computerized bridge circuit consisting of a current source in series with a standard resistor (of better than 1% precision) and the sample. The computer determined the current through the circuit by reversing the polarity of the current and averaging a series of voltage measurements

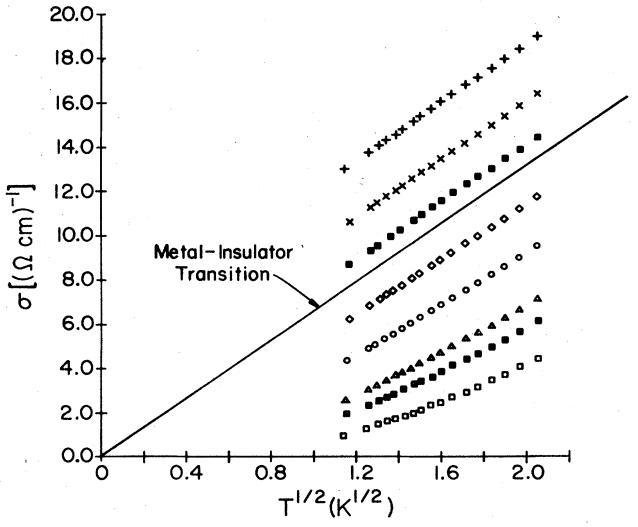

FIG. 6. σ versus $T^{1/2}$ for 1100 Å of $Ge_{0.84}Au_{0.16}$ near the metal-insulator transition. The slopes σ_1 are ~ 6 $(\Omega\,\mathrm{cm})^{-1}\mathrm{K}^{-1/2}$ through the transition. The Mott conductivity is 100 $(\Omega\,\mathrm{cm})^{-1}$.

taken across the resistor. The conductivity was then determined by taking the same sequence of measurements across the sample. These disordered materials exhibit a small voltage-dependent conductivity, so measurements were taken with a constant 20 mV across the sample. Data consist of a series of conductivity-versus-$T^{1/2}$ curves (Fig. 6).

III. RESULTS AND ANALYSIS

Figure 6 shows a series of conductivity curves for 1100 Å of $Ge_{0.84}Au_{0.16}$. These curves roughly obey $\sigma=\sigma_0+\sigma_1 T^{1/2}$ above and through the metal-insulator transition. Insulator effects are evident as the lower curves bend towards the origin.

We computed least-squares fits of the dc conductivity versus temperature data to $\sigma=\sigma_0+\sigma_1 T^{\beta}$. For both Ge_xAu_{1-x} and B_xCu_{1-x}, β ranged between 0.3 and 1.1 approaching $x\sim 0.4$ near the transition, with errors of 10—40 % (Figs. 7 and 8).

We analyzed our data in the context of the two-parameter phenomenological renormalization group theory of McMillan, which includes localization and electron-electron interactions.[14] This theory presents a model into which we can fit our data and extract physical insight. In doing this we realize the theory has questionable assumptions[17] and that conclusions drawn from it must be carefully scrutinized. The theory treats the motion of diffusive electron wave packets at a length scale L. Three length-dependent physical quantities diffusivity D_L, density of states at the Fermi energy N_L, and the dielectric constant ϵ_L, describe the motion of a diffusing electron wave packet of width

$$L=[3\hbar D_L/(\sqrt{2\pi}F_L)]^{1/2},$$

where F_L is the energy spread of the packet. At small length scales the physical quantities change with length scale as described by the differential equations of the renormalization group. At some length scale the system reaches equilibrium and the quantities become constant. Physically, the model describes a microscopic wave packet expanding in real space.[14] At the critical length ξ the packet becomes macroscopic, i.e., conducting, and continues expanding diffusively to infinity. That critical length is the correlation length. Conductivity is defined as $\sigma_L=2e^2N_LD_L$,[18] and the $T=0$ conductivity is $\sigma=\lim_{L\to\infty}\sigma_L$. In the conducting regime the conductivity is

$$\sigma=(0.1)e^2/(\hbar\xi)[1+\xi/L].$$

At finite temperatures the wave packet is destroyed by thermal fluctuations at $L=\xi\sqrt{\Delta/kT}$, where Δ is the energy width of the packet at $L=\xi$. The conductivity is then

$$\sigma=(0.1)e^2/(\hbar\xi)[1+(kT/\Delta)^{1/2}]. \quad (1)$$

The slope of the σ versus $T^{1/2}$ curve is then

$$\sigma_1=(0.1)e^2/(\hbar\xi)(k/\Delta)^{1/2}. \quad (2)$$

At the critical length the width of the wave packet is

$$\xi=[(3/\sqrt{2\pi})\hbar D_\xi/\Delta]^{1/2}. \quad (3)$$

Combining (2) and (3):

$$D_\xi=\text{const}/\sigma_1^2. \quad (4)$$

We computed a least-squares fit to the data for β fixed at $\frac{1}{2}$. The slopes of the $T^{1/2}$ curves, σ_1, which are a manifestation of the system's inelastic interactions, range between 1.0 and 10.0 $(\Omega\,\text{cm})^{-1}\text{K}^{-1/2}$. For Ge_xAu_{1-x} (Fig. 9) the slopes are linear with σ_0 for σ_0 between 10 and 60 $(\Omega\,\text{cm})^{-1}$ and flatten out on both sides of this region. For B_xCu_{1-x} (Fig. 10) the slopes are consistent with a linear relationship with σ_0. Both materials have σ_1 approaching 5.0—10.0 $(\Omega\,\text{cm})^{-1}\text{K}^{-1/2}$ at the transition. The errors in the data are less than 10%. The values of the slopes are consistent with those of Hertel *et al.*,[1] who saw virtually

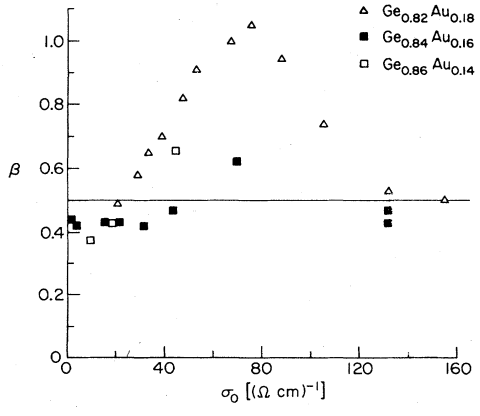

FIG. 7. Power law β of the temperature-dependent conductivity as a function of the distance from the transition of 1000-Å $Ge_{0.82}Au_{0.18}$, 1100-Å $Ge_{0.84}Au_{0.16}$, and 900-Å $Ge_{0.86}Au_{0.14}$ films. The power law approaches 0.40 with 10% error at the transition.

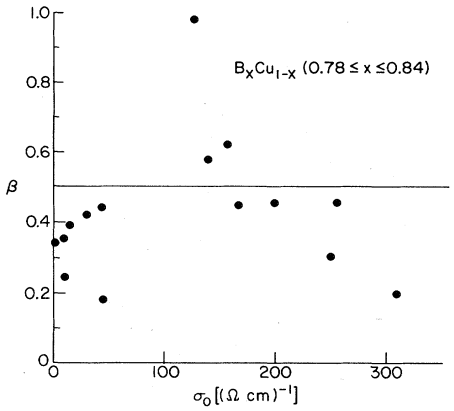

FIG. 8. Power law β of the temperature-dependent conductivity as a function of the distance from the transition of 900-Å to 2400-Å B_xCu_{1-x} films with $0.78\le x\le 0.84$. The power law approaches 0.35 with 10% error at the transition.

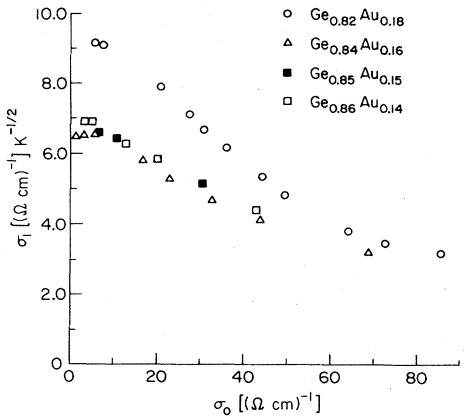

FIG. 9. Coefficient of the temperature-dependent conductivity term σ_1 as a function of distance from the transition of 1000-Å $Ge_{0.82}Au_{0.18}$, 1100-Å $Ge_{0.84}Au_{0.16}$, 900-Å $Ge_{0.85}Au_{0.15}$, and 900-Å $Ge_{0.86}Au_{0.14}$ films. The coefficient is linear with σ_0 for σ_0 between 10 and 60 $(\Omega\,\mathrm{cm})^{-1}$ and flattens out on both sides of this region.

constant slopes of 7 $(\Omega\,\mathrm{cm})^{-1}\mathrm{K}^{-1/2}$ through the transition in their a-Nb:Si temperature data. Cochrane and Strom-Olson[12] also show slopes between 3 and 7 $(\Omega\,\mathrm{cm})^{-1}\mathrm{K}^{-1/2}$ in a variety of amorphous and disordered metals with high conductivities spanning an order of magnitude. These results contrast with the Si:P data[3,4] which have large slopes that seem to diverge at the transition. Interpreting the data in the manner of (4) yields diffusivities at crossover on the order of the free-electron diffusivity, $\hbar/m \sim 1$ cm^2/s, for all of the systems except Si:P. While the slope is a characteristic of inelastic interactions of the electrons, a quantitative interpretation of the significance of D_ξ awaits a more complete model of the system.

The annealing behavior of Ge_xAu_{1-x} prevents the use of gold concentration as the parameter that characterizes the metal-insulator transition. The Drude-electron concentration can be calculated from the Au concentration in a fresh sample, but there is no simple way to determine it after annealing. We chose the bare, i.e., unrenormalized,

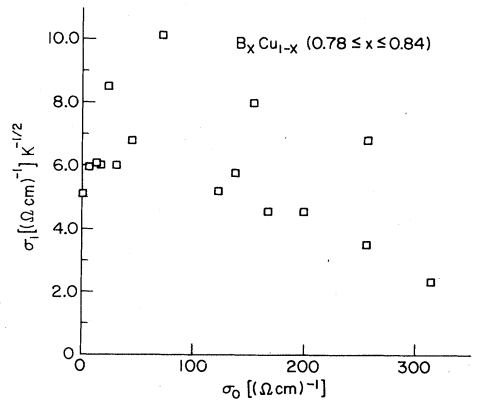

FIG. 10. Coefficient of the temperature-dependent conductivity term σ_1 as a function of distance from the transition of 900-Å to 2400-Å B_xCu_{1-x} films with $0.78 \le x \le 0.84$. The data is consistent with a linear relationship with σ_0.

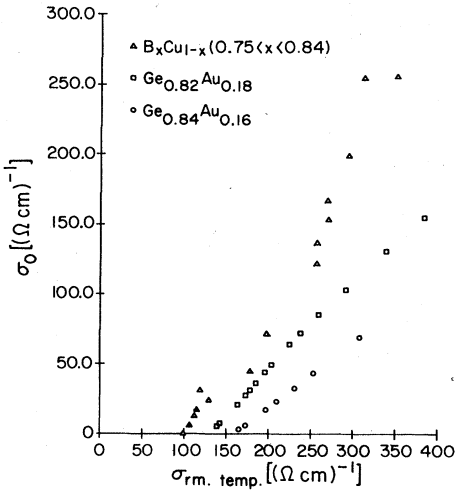

FIG. 11. σ_0 versus $\sigma_{\mathrm{rm\,temp}}$ (the mobility edge) for B_xCu_{1-x} $(0.75<x<0.84)$, $Ge_{0.82}Au_{0.18}$, and $Ge_{0.84}Au_{0.16}$ with power laws of 1.5±0.2, 0.91±0.09, and 1.02±0.15, respectively. The room-temperature conductivity at the metal-insulator transition is $\sim 100\ (\Omega\,\mathrm{cm})^{-1}$, σ_{Mott}.

conductivity as the parameter. The bare conductivity is a reflection of the microscopic length scale, where the system can be treated as free-electron like. A calculation using the simple Drude-model expression relates this conductivity to the electron concentration. In practice, we used room-temperature conductivity as the bare conductivity. In doing so, we assumed that phonons in the system cut the renormalization group off at the same microscopic length scale after each anneal, i.e., the room-temperature electron-phonon scattering time doesn't change.

The shape of the mobility edge was determined by fitting σ_0 from the $\beta=\frac{1}{2}$ fits as a function of room-temperature conductivity. Figure 11 shows the mobility edges for B_xCu_{1-x} $(0.75<x<0.84)$, $Ge_{0.82}Au_{0.18}$, and $Ge_{0.84}Au_{0.16}$. We fit the points to $\sigma_0=A(\sigma_{\mathrm{rm\,temp}}-\sigma_{\mathrm{crit}})^\nu$ which yielded ν's of 1.5±0.2, 0.91±0.09, and 1.02±0.15, respectively. These values are consistent with Hertel *et al.*[1] and Nishida *et al.*[2] and with the predictions of Al'tshuler and Aronov,[13] Al'tshuler *et al.*,[13] and McMillan.[14] The room-temperature conductivity at the transition σ_{crit} is $\sim 100\ (\Omega\,\mathrm{cm})^{-1}$, which equals σ_{Mott}. This is a manifestation of the Ioffe-Regel criterion as the microscopic criterion for the metal-insulator transition. The slopes of the mobility-edge curves depend on microscopic details of each sample. The fact that the B_xCu_{1-x} points lie on a single line indicates that the disorder is independent of initial copper concentration.

We also carried out measurements on a-B_xAu_{1-x}, a-Ge_xAg_{1-x}, and a-Ge_xCu_{1-x}. Their conductivity data showed the same behavior as Ge_xAu_{1-x} and B_xCu_{1-x}.

IV. CONCLUSIONS

We have studied the zero-field transport properties of three-dimensional amorphous Ge_xAu_{1-x} and B_xCu_{1-x} near the metal-insulator transition. These materials can be modeled as disordered metal atoms which supply con-

duction electrons to the system embedded in an inert amorphous matrix. A system's position on the phase diagram relative to the metal-insulator transition is determined by the Fermi energy as mediated by the density of conduction electrons. This density is changed by either clumping of the metal atoms (in Ge_xAu_{1-x}) or by voids in the film (in B_xCu_{1-x}). The conductivity has $\sim T^{1/2}$ dependence near the transition. The coefficient of that temperature term, which is determined by inelastic interactions, has values between 1.0 and 10.0 $(\Omega\,\mathrm{cm})^{-1}\,\mathrm{K}^{-1/2}$, consistent with previous work excluding Si:P. Finally, the data yield mobility edges with power laws of ~ 1, as predicted by McMillan,[14] Al'tshuler and Aronov,[13] and Al'tshuler *et al.*[13] This result shows that the absence of spin-orbit effects does not explain the power law of $\frac{1}{2}$ found for the mobility edge of Si:P.

ACKNOWLEDGMENTS

This work was supported by the National Science Foundation under Contract No. NSF-DMR-83-16981. Sample characterization was carried out in the Center for Microanalysis of Materials, University of Illinois, which is supported by the U. S. Department of Energy under Contract No. DE-AC02-76ER01198.

[1]G. Hertel, D. J. Bishop, E. G. Spencer, J. M. Rowell, and R. C. Dynes, Phys. Rev. Lett. **50**, 743 (1983).

[2]N. Nishida, T. Furubayashi, M. Yamaguchi, H. Ishimoto, and K. Morigaki, Technical Report of the Institute for Solid State Physics, Tokyo, Ser. A, No. 1450 (1984) (unpublished).

[3]M. A. Paalanen, T. F. Rosenbaum, G. A. Thomas, and R. N. Bhatt, Phys. Rev. Lett. **48**, 1284 (1982).

[4]G. A. Thomas, M. Paalanen, and T. F. Rosenbaum, Phys. Rev. B **27**, 3897 (1983).

[5]T. I. Veronina, O. V. Emel'yanenko, T. S. Lagunova, Z. I. Chugueva, and Z. Sh. Yanovitskaya, Fiz. Tekh. Poluproudn. **17**, 1841 (1983); [Sov. Phys.—Semicond. **17**, 1174 (1983)].

[6]T. Chui, P. Lindenfeld, W. L. McLean, and K. Mui, Phys. Rev. Lett. **47**, 1617 (1981).

[7]Z. Ovadyahu, Phys. Rev. Lett. **52**, 569 (1984).

[8]T. F. Rosenbaum, R. F. Milligan, G. A. Thomas, P. A. Lee, T. V. Ramakrishnan, R. N. Bhatt, K. DeConde, H. Hess, and T. Perry, Phys. Rev. Lett. **47**, 1758 (1981).

[9]D. S. McLachlan, Phys. Rev. B **28**, 6821 (1983).

[10]S. Morita, N. Mikoshiba, Y. Koike, T. Fukase, M. Kitagawa, and S. Ishida, J. Phys. Soc. Jpn. **53**, 40 (1984); *ibid.* **53**, 324 (1984).

[11]J. B. Bieri, A. Fert, G. Creuzet, and J. C. Ousset, J. Appl. Phys. **55**, 1948 (1984).

[12]R. W. Cochrane and J. O. Strom-Olson, Phys. Rev. B **29**, 1088 (1984).

[13]B. L. Al'tshuler and A. G. Aronov, Zh. Eksp. Teor. Fiz. **77**, 2028 (1979); [Sov. Phys.—JETP **50**, 968 (1979)]; B. L. Al'tshuler, A. G. Aronov, and P. A. Lee, Phys. Rev. Lett. **44**, 1288 (1980).

[14]W. L. McMillan, Phys. Rev. B **24**, 2739 (1981).

[15]G. S. Grest and P. A. Lee, Phys. Rev. Lett. **50**, 693 (1983).

[16]H. Tardy, Ph.D. thesis, University of Illinois (1985).

[17]P. A. Lee, Phys. Rev. B **26**, 5882 (1982).

[18]In Ref. 17 P. A. Lee points out that N should be replaced with $dn/d\mu$ in the expression for σ_L and that this decouples the scaling equations for the conductance and the interaction constant. Our use of the model, therefore, assumes that the new fixed point is similar in nature to the old one.